

# Particle ID performance of Liquid Argon TPC

J-PARC T32 collaboration

---

## Abstract

This paper describes a study of particle identification performance of liquid Argon TPC (LArTPC) detector using well-defined charged particles (pions, kaons, and protons) with momentum of 800 MeV/c obtained at J-PARC K1.1Br beamline.

We have build a LArTPC detector with fiducial mass of 150 kg, and injected the beam particle

*Keywords:*

---

## **1. Introduction**

Refer [1] for hardware/beam line description

## 2. Data Quality

### 2.1. Collected Data

Table 1 shows list of the collected data while Oct/2010 Run. 800 MeV/c pion is expected to pass-through the detector as MIP, and have uniform energy deposition to all the TPC channels. So this data set is very useful for calibrating the detector response (See section xxx). 800 MeV/c proton stops after 15 cm of flight distance inside the TPC fiducial volume with relatively large  $dE/dx$ . So we use the proton data set for validation of the detector response at high  $dE/dx$  region(See section xxx). We have collected three different Kaon data by varying thickness of the degrader. 540, 630, 680 MeV/c corresponds to the momentum degraded by 2 lead glass, 1 lead glass + 1 lead block, and 1 lead glass, respectively, and such Kaon stops after 10 cm, 50 cm, and 65 cm of flight distance inside TPC fiducial volume.

Figure 1 shows an 2D display of typical event taken with 800 MeV/c electron trigger. Horizontal axis corresponds to TPC channel number and zero means most upper stream strip. Since strip pitch is 1 cm, this is equivalent to distance from beam injection point in cm. Vertical axis corresponds to electron drift time in  $\mu s$  and  $t=0$  means trigger timing. In this TPC, anode and cathode is located at top and bottom of the detector, respectively,  $t=0$  means energy deposition at anode and longer drift time means energy deposition in lower height. With 200 V/cm of electric field, drift velocity is about 0.8 m/ms. So drift of full detector (40 cm) takes 500  $\mu s$ . Color strength of the plot corresponds to the TPC signal pulse height in ADC counts which is roughly proportional to  $dE/dx$  of the track. In this event, triggered electron can be clearly seen center of the detector as an electromagnetic shower while there are two other particles accidentally overlapped with the triggered electron. Track at  $t=100 \mu s$  is considered as a proton which stops after 15 cm of flight distance and has large  $dE/dx$  around the stopped point. Track at  $t=400 \mu s$  is considered as a pion which passes-through the detector and has uniform  $dE/dx$  over the TPC channels. This event already gives us some idea for how good the particle identification performance of the LArTPC is.

Figure 2 shows a typical  $K \rightarrow \mu\nu$  like event. We can clearly identify a kink of the track at 60 cm which is considered as stopped point of Kaon and it decays to

Energy deposition of the track is about MIP at the injection point and gradually increase towards the stopped point at 60 cm.

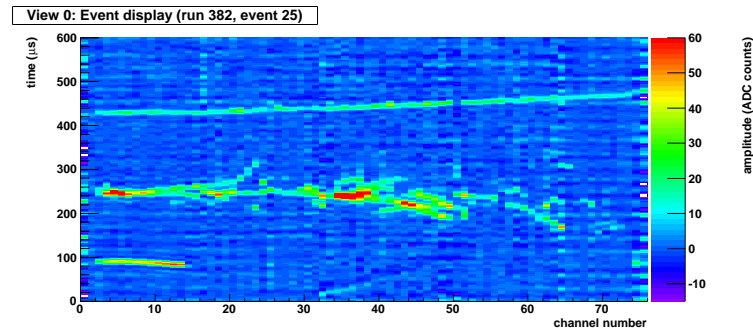


Figure 1: Event display of 800 MeV/ $c$  electron triggered event. Accidentally overlapped with a proton and a pion.

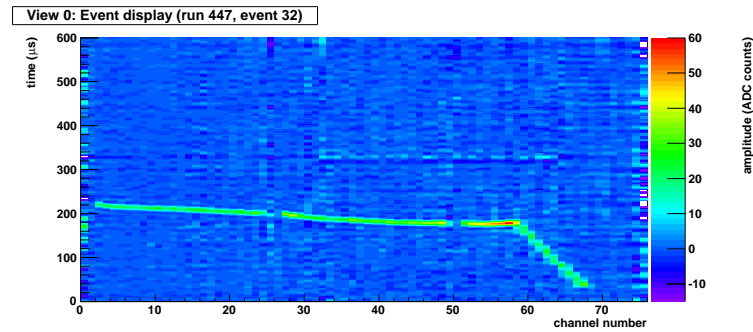


Figure 2: Event display of Kaon 630 MeV/ $c$  triggered event

Table 1: List of collected data

Particle	Momentum (MeV/c)	Number of Events
Pion	800	3,000
Proton	800	1,500
Kaon	540 (2LG)	7,000
Kaon	630 (1LG+1LB)	40,000
Kaon	680 (1LB)	35,000
electron	800	2,500
electron	200	10,000
pion	200	10,000

Table 2: Detector response

Particle	FC(K)	FC( $\pi$ )	GC
$\pi^+$	x	o	x
$K^+$	o	x	x
$p$	x	x	x
$e^+$	x	o	o

## 2.2. Beam Quality(Purity)

We have several beam counters to identify beam particles event by event (see Fig3). Beam includes  $K^+$ ,  $\pi^+$ ,  $e^+$  and  $p$  which have the momentum adjusted  $\sim 800\text{MeV}/c$ . We need to obtain  $K^+$ ,  $\pi^+$  and  $p$  events and to reject  $e^+$  events for analysis. Fitch Cherenkov Counter is the differential-type detector which can select  $K^+$  and  $\pi^+$  with differences of angle of cherenkov light emitted. As shown Fig4, the response of Fitch Cherenkov Counter are categorized into three,  $K^+$  like events,  $\pi^+$  or  $e^+$  like events and  $p$  like events. Why  $\pi^+$  like events and  $e^+$  like events are same category is the velocities of both particles are very close. Gas Cherenkov Counter is the threshold-type detector which can select  $e^+$  because only  $e^+$  can emitted cherenkov light in the gas of the detector. Figure5 shows the response of Gas Cherenkov Counter, and we define the events GC signal are above dashed line as  $e^+$  events. Table2 shows whether the particles leave signals on each detector.

As shown Table2, we can select beam particles into above four particles by using the information of Fitch Cherenkov Counter and Gas Cherenkov Counter. In addition, we can increase the purity of each particles by using

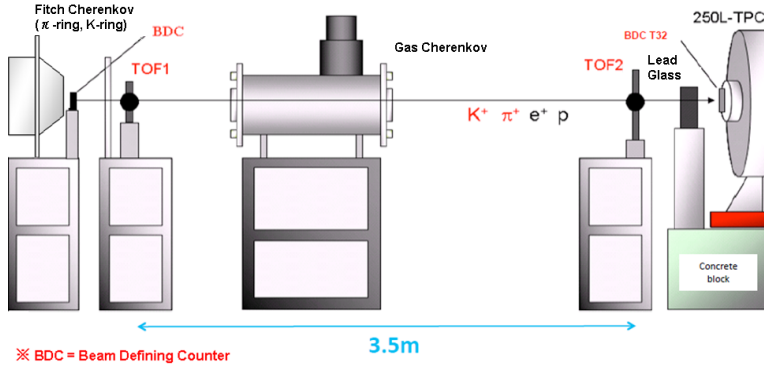


Figure 3: Instruments on K1.1BR Beam Line

Table 3: Time of flight of each particle

particle	$e^+$	$\pi^+$	$K^+$	$p$
Mass(MeV)	0.511	139.57	493.68	938.27
Time of Flight(ns)	11.67	11.84	13.71	17.98

the information of TOF Counter. There are two TOF Counters which has  $\sim 200$  ps resolution 3.5m apart, and each particle are selected with the difference of time of flight between them. Table3 is calculated time of flight when each 800MeV/c particle passes two counters. As table3 shows,  $e^+$  and  $\pi^+$  cannot selected because the difference of time of flight is too short for the TOF resolution. Figure6 shows the response of TOF Counter, and they are categorized into three,  $\pi^+$  or  $e^+$  like events,  $K^+$  events,  $p$  events. Herewith we can obtain high-purity samples of each particle by using the information of Fitch Cherenkov Counter, Gas Cherenkov Counter and TOF Counter. Especially, We have obtained  $K^+$  events for  $K^+$  run by requiring the condition  $FC(K)$  signal is above 2000 as trigger. Figure7 shows the response of TOF Counter after required the above condition. Even though a few events which are defined as  $K^+$  like events at Fitch Cherenkov Counter exude  $\pi$  event region at TOF Counter, we can reject those events by using this information and obtain  $K^+$  samples of  $\sim 100\%$  purity. Table4 shows particle fraction of samples used for analysis.(Total number of all four particles is 100)

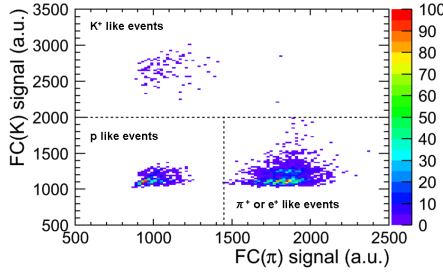


Figure 4: Fitch Cherenkov Counter

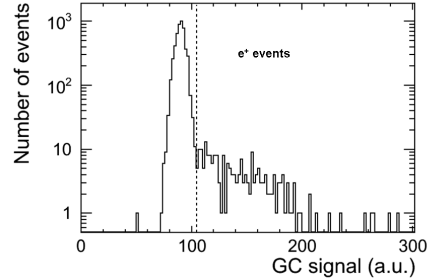


Figure 5: Gas Cherenkov Counter

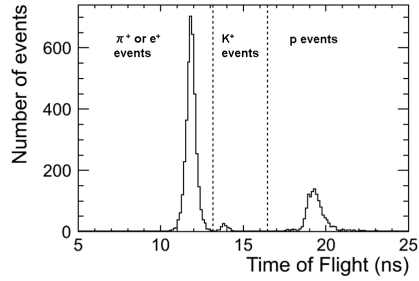


Figure 6: TOF Counter

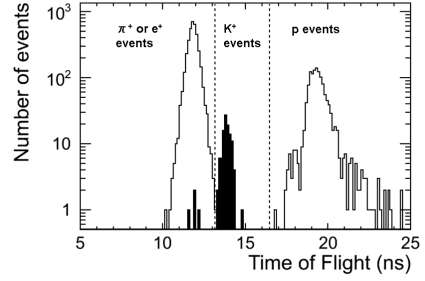


Figure 7: TOF Counter after cut

Table 4: Beam components

	$e^+$	$\pi$	$K^+$	$p$
Pion run	5	83	3	9
Proton run	0	23	0	77
Kaon run	0	0	100	0

### 2.3. Beam Energy

#### 2.3.1. Kaon energy

Time resolution of TOF counters is not enough to determine Kaon beam energy. Kaon beam energy is estimated by comparing decay point distribution of data and MC simulation as described in section 6.8.1.

#### 2.3.2. Proton energy

Since proton mass is relatively heavy, proton energy is determined by TOF counters information. Figure 8 shows  $\Delta\text{TOF}$  distribution of TOF counters. Figure 9 shows proton momentum estimated by TOF counters information.

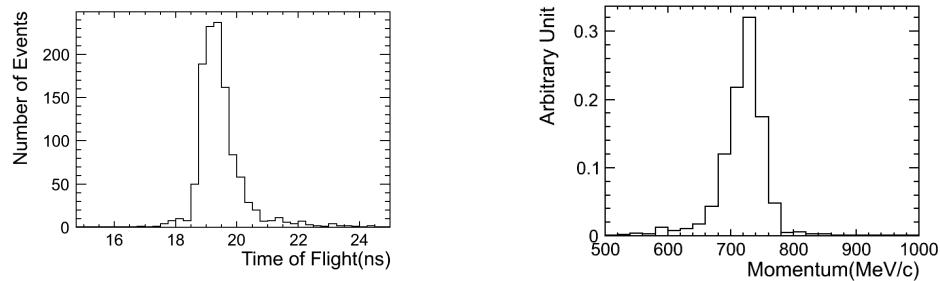


Figure 8:  $\Delta\text{TOF}$  distribution of TOF counters with proton data

Figure 9: proton momentum estimated by  $\Delta\text{TOF}$  of TOF counters information

### 2.4. Beam Position

We measured beam profile in front of 250LAr TPC beam window by using plastic scintillation counters. Figure 10 shows beam profile result.

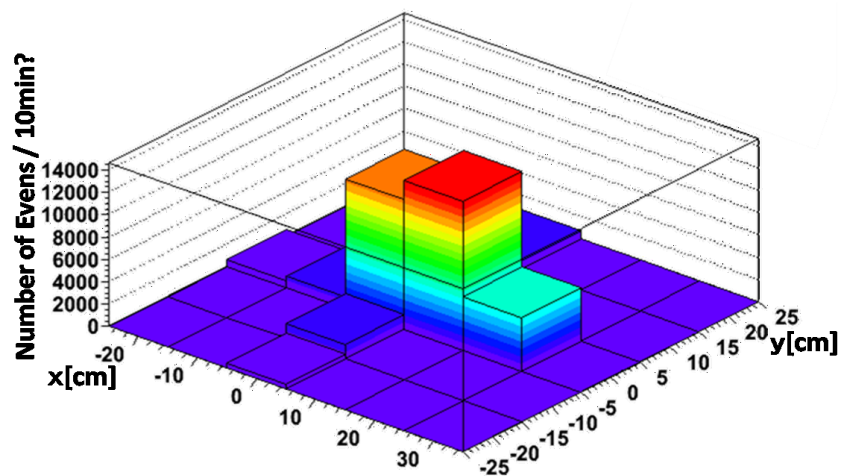


Figure 10: Beam profile on the front of 250LAr TPC

### **3. Software Framework**

Qscan is a general purpose software package for LArTPC analysis(reference) which provides,

- event reconstruction: noise reduction, hit finding, clustering, and tracking...
- event simulation: GEANT VMC with ROOT geometry, ionization electron recombination, drift, digitization...
- event visualization: display raw data waveform and reconstructed quantities

## 4. Event Reconstruction

### 4.1. Noise Reduction

Figure 12 shows raw waveform of the TPC signal before applying any noise reduction. Two waveforms shown in this plot are channel 13 and 37 in Figure 1 which are roughly proton stopped point and electron shower maximum point, respectively. Signal-to-noise ratio for this particular case is poor and pion signal which is supposed to be  $t=400 \mu\text{s}$  is almost hidden by the noise. While time width of TPC signal is few  $\mu\text{s}$  which is determined by drift time between anode and anode-grid, dominant noise component looks higher frequency. To reduce such noises, we have applied FFT (Fast Fourier Transformation) filter to cut the high frequency component. Figure ?? shows amplitude as a function of frequency for the same event. This clearly shows dominant noise component with  $> 200 \text{ kHz}$  has good separation with signal component ( $< 100 \text{ kHz}$ ). Figure 13 shows the waveform after removing high frequency ( $> 80 \text{ kHz}$ ) component by the FFT filter. Signal-to-noise ratio is dramatically improved. On the other hand, we expect certain bias to the signal charge measurement by this filter, and it will be discussed in Section X.

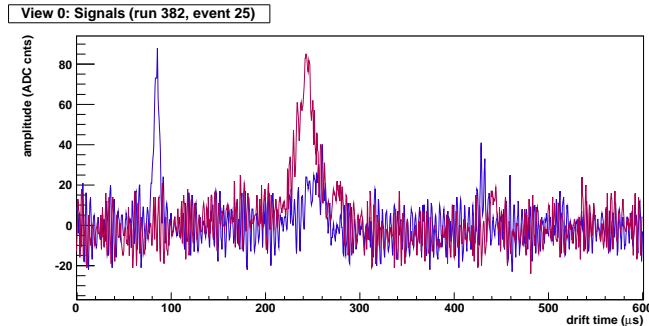


Figure 11: TPC raw signal waveform for "Textbook" event channel 13 and 37.

### 4.2. Hit Finding/Clustering

After noise reduction we find signal hits and create clusters associated to single tracks. Hit is defined as bump over given threshold in a channel. After finding all hits in an event, we construct cluster by merging adjacent hits. The example of hit finding and clustering is shown in Fig 14, which

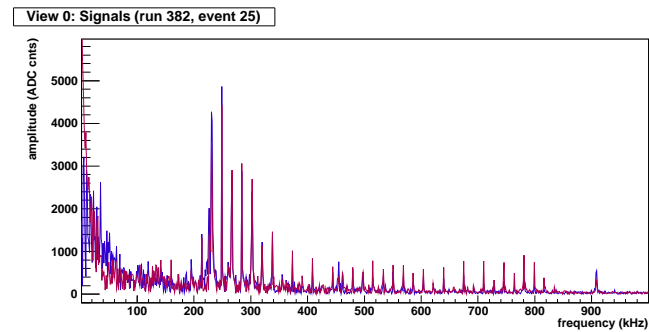


Figure 12: FFT frequency amplitude distribution

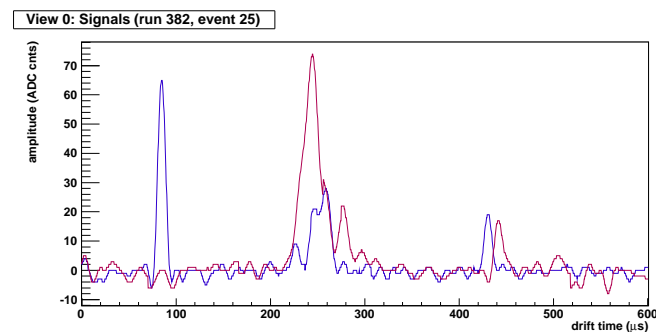


Figure 13: TPC signal waveform after cutting the frequency > 80 kHz.

indicates reasonable hit and cluster findings. Threshold of hit finding is 6 ADC counts, which is about  $2.5\sigma$  from typical data noise level (as shown in Fig 12) and keeping more than 99% of Kaon hit finding efficiency from simulation. ADC count distribution is fitted by step function plus Gaussian to estimate the charge of hit in  $\text{ADC} \times \mu\text{s}$  unit. Fitting  $\chi^2 < 3$  and  $2.5 < (\text{time width of hit}) < 8 \mu\text{s}$  are required to remove noise hits further.

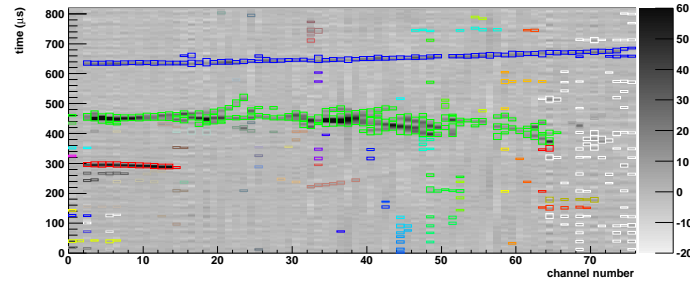


Figure 14: Example of hit finding and clustering. A colored box corresponds to a hit and colors represent different clusters.

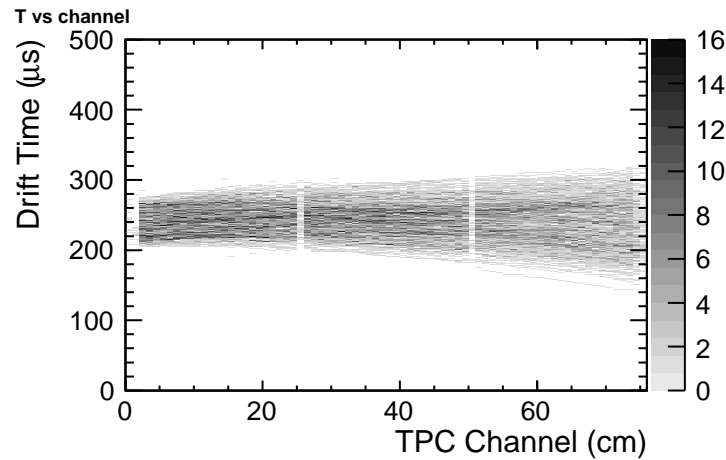


Figure 15: 800 MeV/c pion sample

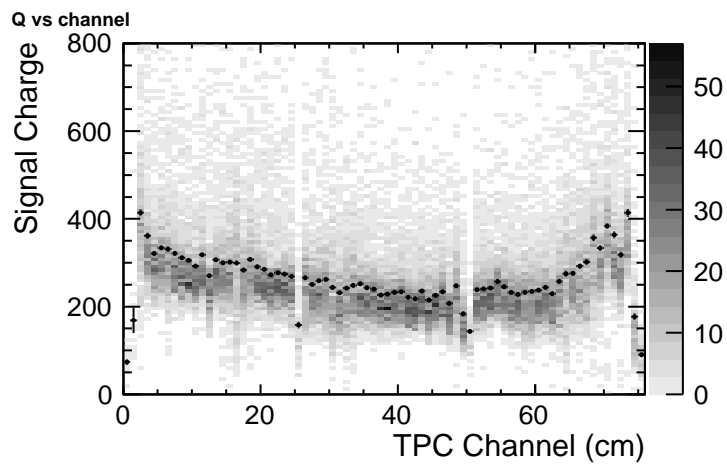


Figure 16: 800 MeV/c pion average hit charge

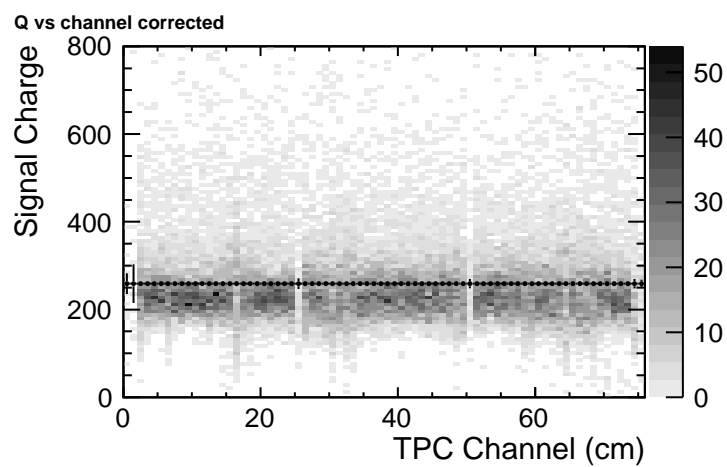


Figure 17: 800 MeV/c pion average hit charge after calibration

### *4.3. Stopped Point Finding*

#### *4.4. Stopped Kaon*

Hough transform was invented for machine analysis of bubble chamber photographs by Paul.V.C.Hough.[6] We find straight lines using hough method , and find Kaon stopped point from the intersection of straight lines. Figure 18 shows hit map like a Kaon track. One point in the X-Y space can be transformed into sinusoidal curve in the  $\rho$ - $\theta$  space. Figure 19 shows sinusoidal curves in all points. And, we find the straight line associated with the largest number of points by choosing the most dense point in  $\rho$ - $\theta$  space. Next , the sinusoidal curves of the hits associated with frist straight line are removed from figure 19. Figure 20 shows sinusoidal curves after the hits associated with frist straight line removed. We find second straight line using the same procedure. This procedure is repeated until there are less than three points. Figure 21 shows the two straight lines found by hough transform mehodt.

Kaon stopped point in the liquid argon detecor defined as charge maximum point around the intersection of some lines.

##### *4.4.1. Chi2 method*

$\chi^2$  method is the algorithm that search the point of rapidly increasing fit'  $\chi^2$  and the point defined as the stopped point. Because the charged particle coming from upstream of beam line , track reconstruction is started from minimum channel to the maximum channel of the cluster.

Figure 22 shows hit map like a Kaon track. We start fitting with straight line from minimum channel to maximum channel. Figure 23 shows range vs fit'  $\chi^2$  distribution. As it can be noiced for figure 23,  $\chi^2$  is increased rapidly if the straight line is strayed out. Then , we search the strayed point from the straight line by setting reasonable threhold and draw from minimum chan- nel to the strayed point. This procedure is done from maximum channel to minimum channel in the same way. And we draw from maximum channel to the strayed point. Kaon stopped point in the liquid argon detecor defined as charge maximum point around the intersection of two lines.

##### *4.4.2. BS method*

In the  $\chi^2$  method , we can't find Kaon stopped point in the case of backward decay. Then , we find Kaon stopped point using BS method.

BS method is concept that the Kaon stopped point defined as lightmost channel in the case of backward decay. we descript below how the track

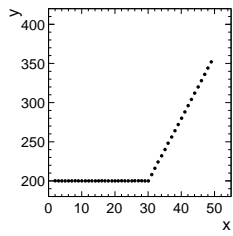


Figure 18: Hit map like a Kaon track

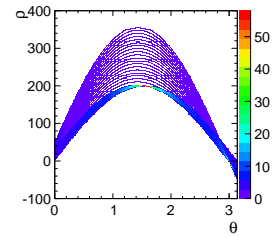


Figure 19: sinusoial curves getting form all hough transformed points of Figure 18

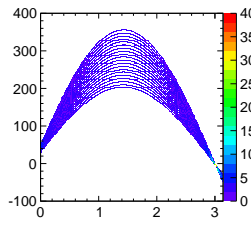


Figure 20: sinusoial curves removed the points associated with first straight line from figure 19

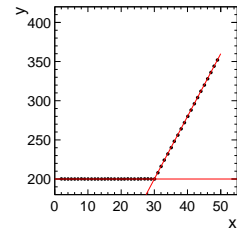


Figure 21: Two lines found with hough transform method

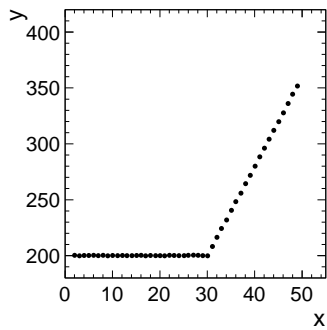


Figure 22: hit map like a Kaon track

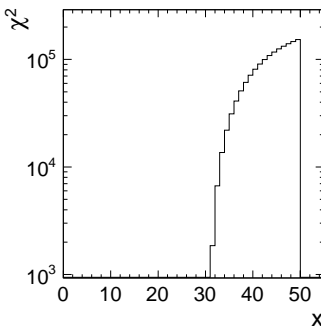


Figure 23: range vs  $\chi^2$  distribution

defined as backward decay.  $N_1$  is defined as Number of cluster hits found by the clustering. Stopped point finding is started from minimum channel. We search for the closet timing hit in next channel from current channel

hit. Then , we repeat this procedure until maximum channel and count the number of selected hit information( $N_2$ ). In the case of backward decay ,  $N_1$  is larger than  $N_2$ . So , we set reasonable threhold of the difference between  $N_1$  and  $N_2$  , and if the  $N_1 > N_2$  is over the threshold , the track is defined as backward decay. In the case of backward decay , we defined charge maximum point around the maximum channel as the stopped point.

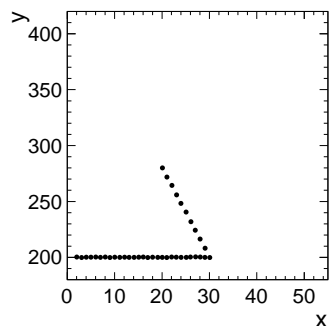


Figure 24: hit map like a Kaon track

## 5. Liquid Argon Purity

Attenuation of the drift electron depends on purity of LAr since electronegative impurities capture it [5]. Thus we need to apply correction to TPC signal charge depends on the drift time. We use cosmic ray sample triggered by inner PMT at off-beam timing for measuring the LAr purity, and use this to correct the beam data. Figure 25 shows an event display of typical cosmic muon event across TPC channels. The attenuation of readout charge depending on drift time is clearly seen in the right plot. Readout charge in an event cannot be fitted by exponential because energy deposition follows Landau distribution and charge readout is affected by electric field distortion which is described latter in section ??.

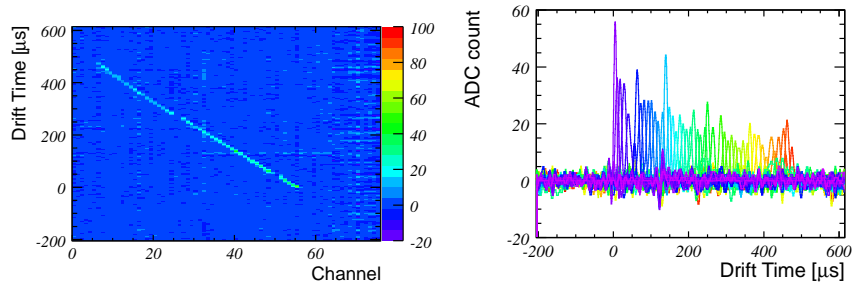


Figure 25: Left: Typical cosmic muon event across TPC channels. Right: Charge deposit as a function of drift time. Colors correspond to different TPC channels.

We select cosmic ray event with more than 20 TPC channels which corresponds to zenith angle of more than  $27^\circ$  and consistent with straight line by  $\chi^2$  fit. Readout charge is corrected for field distortion and projected to beam direction to correct injection angle. We fit readout charge by Landau function in each drift time bin to estimate average charge deposit. Figure 26 shows example of the average readout charge as a function of drift time which is fitted by exponential to obtain drift electron lifetime. Realistic Monte Carlo simulation shows about 13% (TBU) smaller lifetime estimation due to noise, field distortion, and FFT effects. We correct output lifetime from these effects. Figure 27 shows an drift electron lifetime as a function of duration after initial LAr filling. Drift electron lifetime was  $600 \mu\text{s}$  at 60 hours, and  $400 \mu\text{s}$  after 150 hours. The degradation is possibly due to impurity from micro

leak or out-gassing penetrating faster than purification by gas recirculation. But we kept enough drift electron lifetime during data taking period.

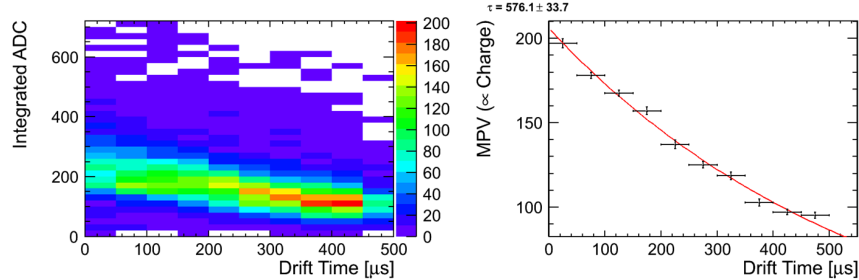


Figure 26: TBU. Left: Readout charge as a function of drift time. Readout charge in each drift time bin is fitted by landau function. Right: Average charge readout as a function of drift time which is fitted by exponential to estimate drift electron lifetime.

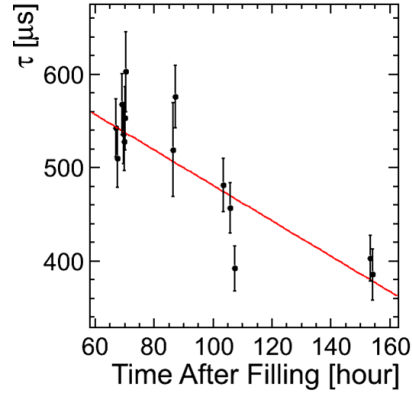


Figure 27: TBU. Drift electron lifetime as a function of duration after initial LAr filling. The lifetime is used to correct the beam data.

## 6. Event Simulation

### 6.1. Geant3, recombination, drift velocity

We use GEANT3 for simulating energy deposition of initial beam particles and secondary particles to LArTPC detector and beamline counters.

we set the maximum step of Geant to 0.5 mm which is enough smaller than the readout pitch of 1 cm. It means charge deposition in one strip is typically simulated with 20 GEANT steps.

We set energy cut-off for soft electron/photon emission to 10 keV which is minimum possible energy can be set in GEANT3. This cut-off is very important for ionization electron recombination.

Recombination of electron and Argon ion depends on the electric field and  $dE/dx$ . We use a measurement in Ref.[3].

$$Q = A \frac{Q_0}{1 + kdE/dx}, A = 0.800, k = 0.486 \quad (1)$$

Velocity of the drift electron depends on the liquid Argon temperature and the electric field. We use a measurement in Ref [4].

- Plot: Geant Geometry, typical track (Tanaka)
- Plot: recombination factor, drift velocity (Tanaka)

### 6.2. Electric Field

Electric field of the TPC field cage We have calculated the electric field using a 2D FEM (Finite Element Method) package [? ].

This field map is used for simulating electron drift.

### 6.3. Drift Electron Diffusion

- Plot: drift simulation (Tanaka)

### 6.4. Preamp Gain Calibration

- Preamp gain vs channel number (Naito)

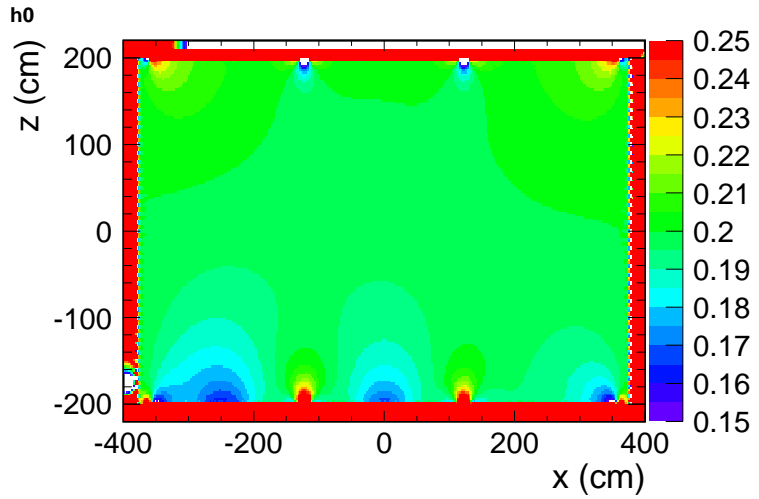


Figure 28: Electric field map obtained from 2D FEM calculation

### 6.5. FFT Noise

There are two kinds of noise in the data we obtained, random noise and coherent noise. Random noise is the noise which exists in each anode channel. Coherent noise is in each board. The pseudo noise we implemented in Monte Carlo simulation is composed of random and coherent noise by this reason.

Random noise is generated from FFT(Fast Fourier Transform) distribution of real data. Figure 29 shows an example of FFT distribution.

Coherent noise is generated board by board as the noise scale in the real data we obtained. The noise scale is defined as a root mean square of pedestal, minimum noise scale is about 3 and maximum noise scale is about 10 in the data.

The ratio of random and coherent noise is 1:1 as equation 2. Figure 30 shows real data noise and Fig.31 shows pseudo noise we implemented in Monte Carlo simulation.

$$Pseudo\ Noise = \frac{Random\ Noise + Coherent\ Noise}{2} \quad (2)$$

- Plot: simulated event (Nagasaki)

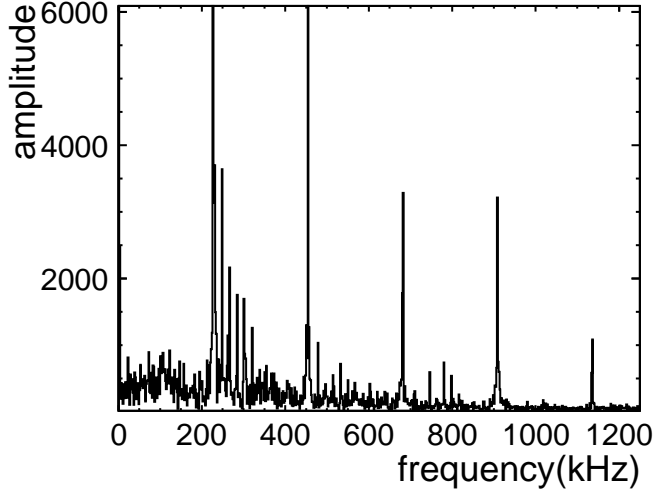


Figure 29: An example distribution of frequency

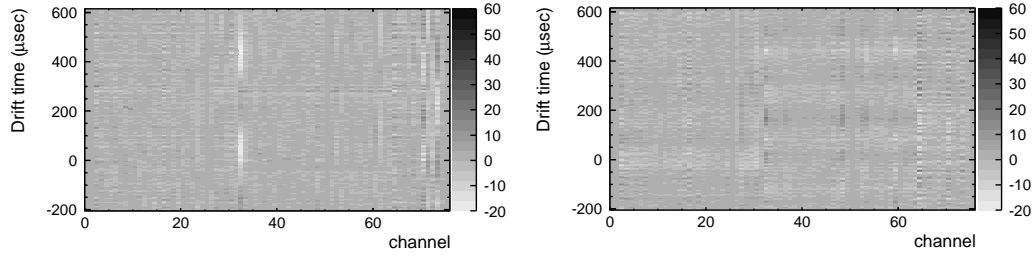


Figure 30: Data noise

Figure 31: Pseudo noise(Noise simulation)

### 6.6. Cross Talk

Figure 32 shows the signal wave form of stopped channel and the front channel of typical proton event. The signal wave form of stopped channel is differential form of the that of the front channel. Such signals are appeared at channel number 1 which cannot enter drifted ionization electron in electric power lines. One possibility which cause such a phenomenon is following process. The distance between anode channels is very short, so the influence of mutual capacitance become large and this capacitive coupling induce cross talk noise. This effect notably appears the channel where the difference of the charge between adjacent channels is large, such as the channel around stopped point of proton. Then, we implement this phenomenon in Monte

Carlo Simulation by adding bipolar shape of the signal Gavin shape at adjacent channels. The area of the mountain of bipolar shape is 10.5% of the area of signal gaussian at each adjacent channel. The value of 10.5% is determined by comparing the hit charge distribution at stopped channel between data and MC simulation. Figure33 shows hit charge distribution of stopped channel. Black is data and blue is MC simulation with cross talk red is MC simulation without cross talk. As fig33 shown, data and MC simulation with cross talk is good agreement, so the value of 10.5% is reasonable.

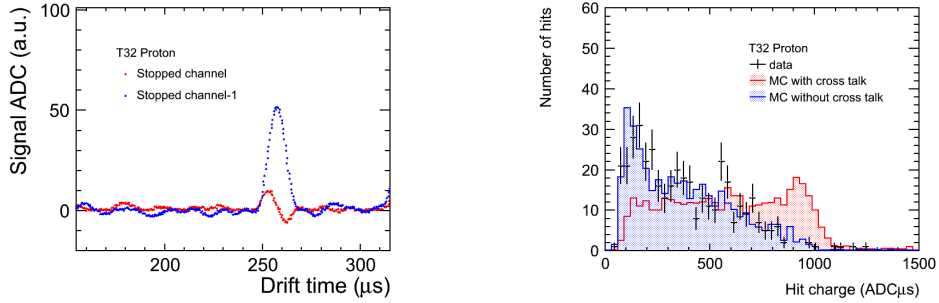


Figure 32: Signal wave form of stopped channel and the front channel

Figure 33: Hit charge distribution of stopped channel

- Plot: signal waveform (proton stopped point + 1) (A. Okamoto)
- Plot: simulated event with and without cross talk (A. Okamoto)

### 6.7. Signal and Noise Scale Tuning

- Plot: Landau distribution after the tuning (Tanaka)

### 6.8. Beam energy

We estimated a beam momentum using simple MC simulation. Figure 34 shows MC simulation's geometry. We generate 800MeV/c pencil beam and shoot the beam downstream. Figure 35 shows Kaon and Pion momentum distribution using this MC simulation at BDC. Kaon beam momentum is estimated by the momentum distribution of MC simulation.

#### 6.8.1. Kaon energy

Kaon beam momentum is estimated by the momentum distribution of MC simulation. We change Kaon beam momentum in a range of 700 - 800 MeV/c and search the momentum that decay point distribution of MC simulation is consistent with data one.

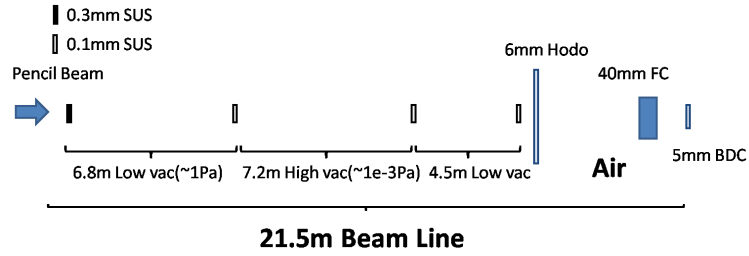


Figure 34: K1.1 Br beam line

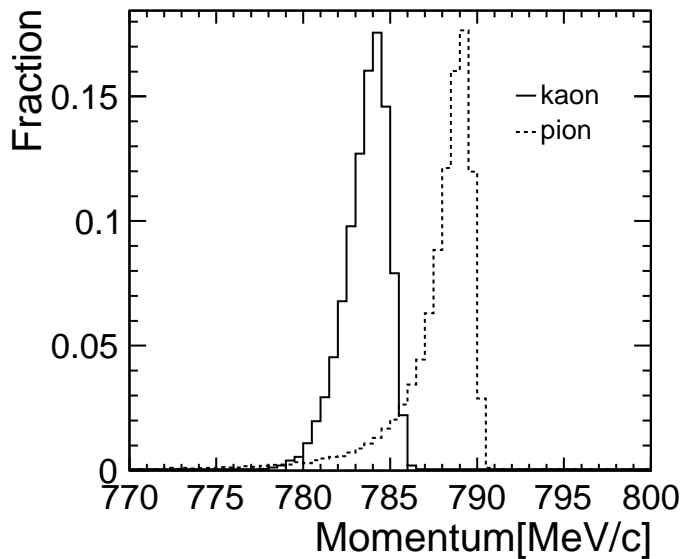


Figure 35: Kaon and Pion momentum distribution at BDC

### 6.8.2. Proton energy

Proton momentum shown in Figure 9 is used as proton beam momentum of MC simulation.

### 6.8.3. Energy deposition in degrader

It is too high energy that Kaon beam stops in the fiducial volume of 250LAr TPC. In order to degrade the beam momentum, some lead glass blocks and a lead brick were inserted in front of 250LAr TPC as degrader. Figure 36 shows energy deposition distribution in degrader.

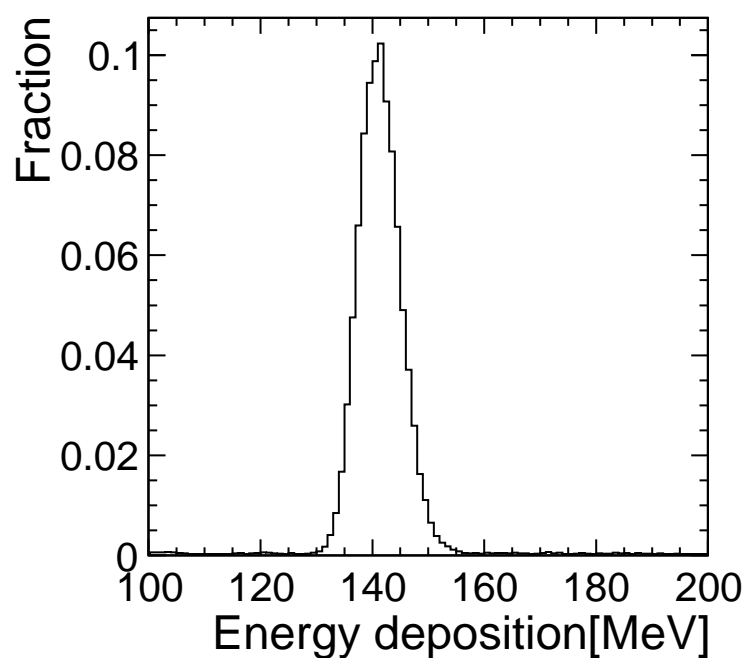


Figure 36: Energy deposition in degrader

## 7. Data- MC Comparison

### 7.1. Through-going Pion

- Plot: Data-MC comparison (Tanaka)

### 7.2. Stopped Proton

Protons are selected by the information of beam counters. Proton events are applied following simple selections. The drift time of the hit at the injection point are restricted from  $150\mu\text{s}$  to  $300\mu\text{s}$  which corresponds with BDC fiducial volume. The total hit number in the cluster is greater than 5. Only one hit are required at the same channel in the cluster to remove multi-track events. Then, we define the events which the number of clusters in the event which passed above selections is only one as good proton events. For good proton events, we compare each parameter between data and MC. Figure?? shows the comparison of the distribution of Hit Charge, Hit Sigma, Stopped Channel and Cluster Charge between data and MC. All four distributions of MC reproduce data well. Especially, the agreement of stopped channel distribution shows the consistent the momentum estimation by TOF information with the initial momentum of the particles injected to 250L detector.

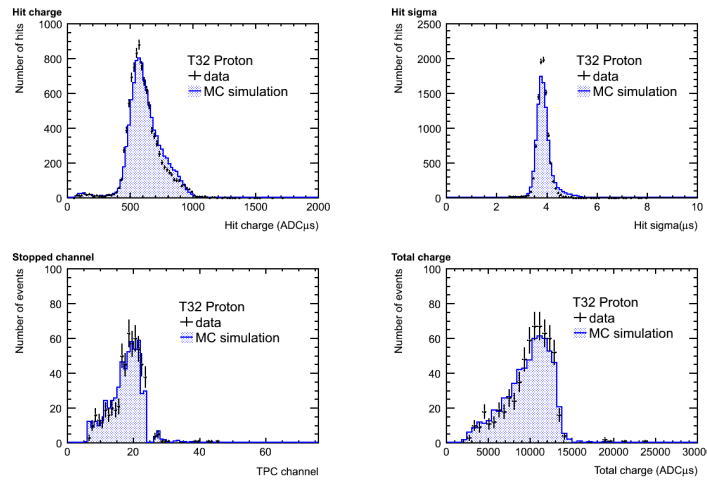


Figure 37: Hit Charge, Hit Sigma, Stopped Channel, Cluster Charge

Figure38 shows the hit charge distribution of each distance from stopped point. Hit charge distributions of MC simulation are good agreements with

data.

Figure 39 shows the mean of the above distribution of each distance. Figure 40 shows the ratios of Data/MC. The ratios are within 94%~105%. From this result, MC simulation reproduce the charge response of data in high and wide dE/dx region well.

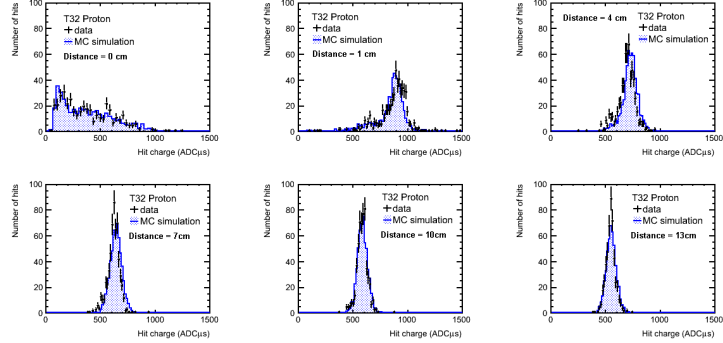


Figure 38: Hit charge distribution of each distance from stopped point

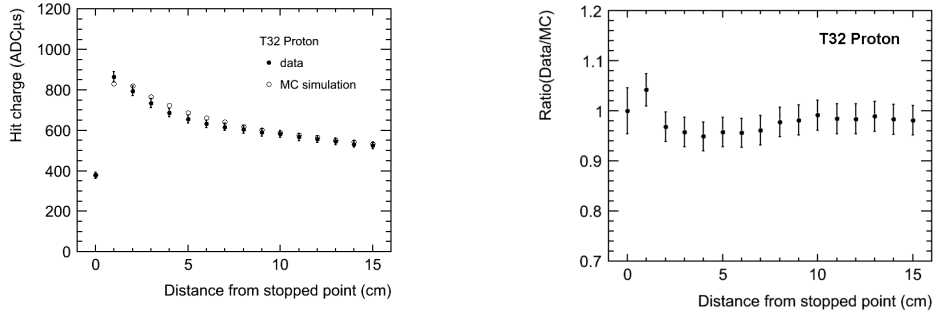


Figure 39: Data-MC comparison of the mean of hit charge distribution

Figure 40: Data-MC comparison of the ratio of the mean

### 7.3. Recombination Factor

Electron-ion recombination depends on the electric field and stopping power  $dE/dx$ . We study this factor using tagged proton beam. Recombination factor measurement using proton beam is relatively easy because of stability of proton. This is why we used proton beam for this study as a first

step.

Expression for recombination can be derived

$$Q = A \frac{Q_0}{1 + (k/E) \times (dE/dx) \times (1/\rho)} \quad (3)$$

where  $Q_0$  is initial ionization charge,  $E$  is electric field,  $dE/dx$  is energy deposit per distance,  $\rho$  is density of liquid Argon,  $A$  and  $k$  are fit parameters. This formula can be rearranged like below:

$$\frac{Q_0}{Q} = \frac{1}{A} + \frac{(k/E)(dE/dx)(1/\rho)}{A} \quad (4)$$

The ratio of  $Q_0/Q$  depends on stopping power  $dE/dx$ , so we determined fit parameter  $A$  and  $k$  using proton data and Monte Carlo simulation. In this analysis, we need  $Q$ ,  $Q_0$  and  $dE/dx$  channel by channel. First, electric field  $E$  was 200 V/cm in our test. Second,  $Q$  is integrated charge in an anode readout channel. Third,  $Q_0$  is integrated charge without recombination factor in an anode readout channel. And then,  $dE/dx$  per an anode channel is determined with truth information of Monte Carlo simulation. Figure 41, 42, 43 show  $Q$ ,  $Q_0$ ,  $dE/dx$  as a function of distance from stopped channel between 1 to 14 channel.  $Q$  is obtained from data,  $Q_0$  and  $dE/dx$  are obtained from Monte Carlo simulation. In many case, integrated charge in stopped channel are more affected by noise from next channel. This is the reason why we don't use information from stopped channel in this analysis.

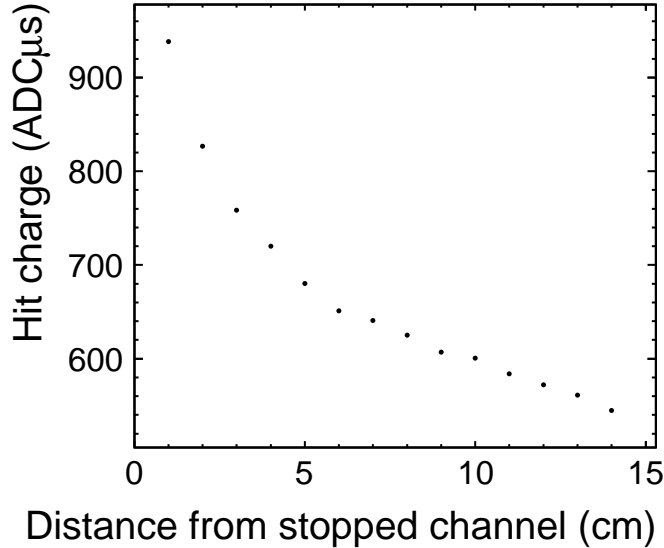


Figure 41: DATA:Integrated Flash ADC counts from stopped channel -1

The result of this study is shown in Fig44. Vertical axis is  $Q_0/Q$ , and horizontal axis is  $dE/dx$  in this figure, this plot is fitted by Birks law. As a result, we got fitting parameter

$$\begin{aligned} A &= 0.832 \pm 0.009(\text{stat.}) \pm 0.006(\text{syst.}) \\ k &= 0.0504 \pm 0.0010(\text{stat.}) \pm 0.0013(\text{syst.}) (\text{kV(g/cm}^2\text{)/cm/MeV}) \end{aligned} \quad (5)$$

We checked Birks law in the range  $4 \text{ MeV/(g/cm}^2\text{)} \leq dE/dx \leq 12 \text{ MeV/cm}^2$  and the result is consistent with ICARUS experiment's one[3] in – sigma.

#### 7.4. Stopped Kaon

In this section, we compare some quantities of data and MC simulation that K stops in the liquid argon detector and we can find stopped point. Figure 45 shows Data and MC comparison for signal hit charge, signal width, decay point and total particle charge distribution. Data of signal charge and signal width are consistent with MC one in error by less than two % and data of cluster charge and primary charge are consistent with MC one in error by less than five %.

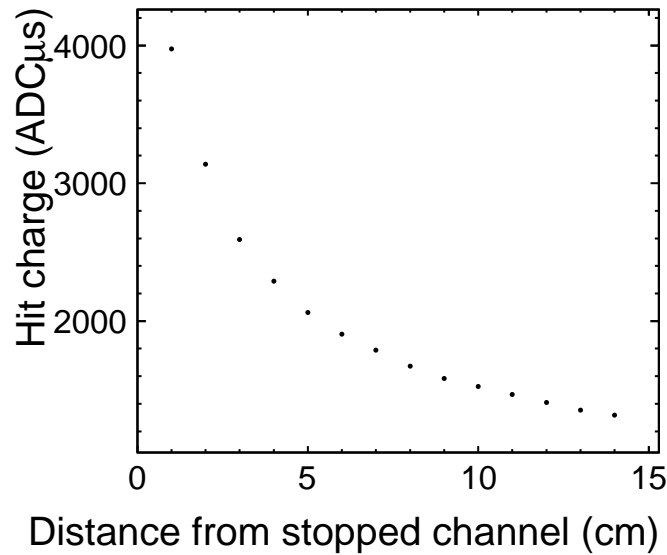


Figure 42: MC without recombination: Integrated Flash ADC counts from stopped channel -1

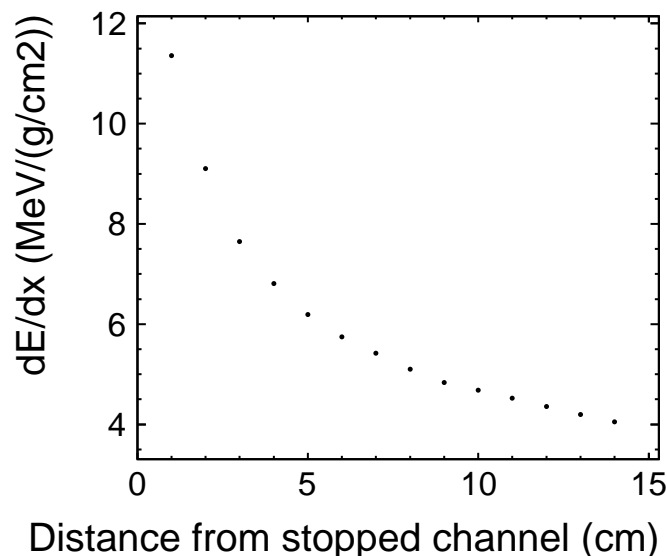


Figure 43:  $dE/dx$  from stopped channel -1

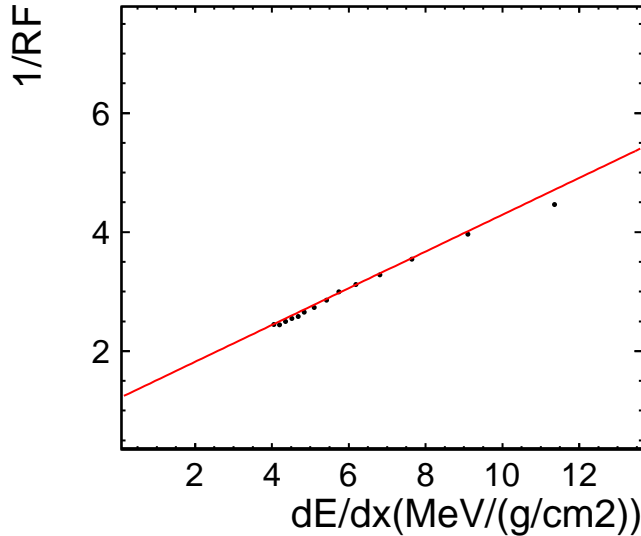


Figure 44: 1/RF VS  $dE/dx$ : fitted by Birks law

Figure 7.4 shows signal hit charge distribution of restricted channel 27. As shown in figure 7.4, signal charge have two peaks at 300 and 500 ADCus. Because two peaks has correlation of  $\Delta$ TOF, possible assumption of the cause is that beam line were bipolarized and the beam didn't pass in the center of the detector. So, we use only the event that signal charge of restricted channel 27 is less than 350. Figure 47 shows signal hit charge distribution in different distance from the stopped point.

As shown in figure 47, data is consistent with MC one. Figure 49 shows data/MC ratio of signal hit charge distribution in different distance from the stopped point. Data of signal charge in different distance from stopped point are consistent with MC one with in 5%.

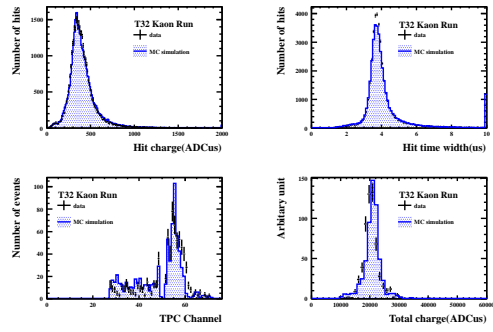


Figure 45: Data-MC comparison for hit charge, hit sigma, cluster charge, primary particle charge

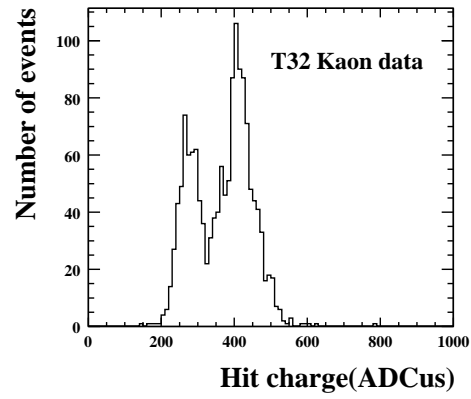


Figure 46: Hit charge in channel 27

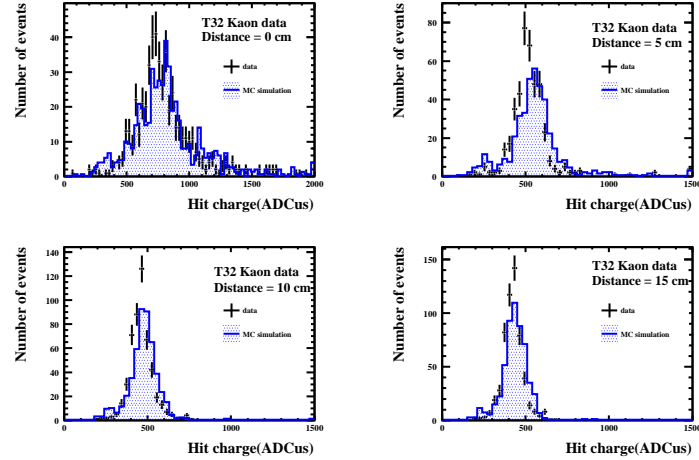


Figure 47: Data-MC comparison for hit charge distribution in different distance from the stopped point (top left: decay point, top right: decay point-5cm, bottom left: decay point-10cm, decay point-15cm)

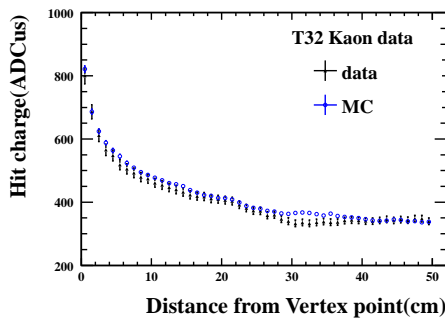


Figure 48: Data-MC comparison for hit charge distribution in different distance from the stopped point

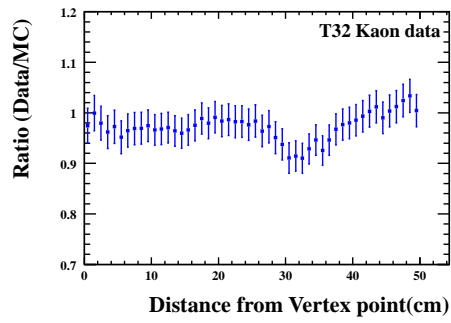


Figure 49: Data/MC ratio for hit charge distribution in different distance from the stopped point

## **8. Summary**

## References

- [1] O. Araoka *et al.*, J. Phys. Conf. Ser. **308**, 012008 (2011) [arXiv:1105.5818 [physics.ins-det]].
- [2] S. Mihara [MEG Collaboration], Nucl. Instrum. Meth. A **518**, 45 (2004).
- [3] S. Amoruso *et al.* [ICARUS Collaboration], Nucl. Instrum. Meth. A **523**, 275 (2004).
- [4] S. Amoruso, M. Antonello, P. Aprili, F. Arneodo, A. Badertscher, B. Baibusinov, M. Baldo-Ceolin and G. Battistoni *et al.*, Nucl. Instrum. Meth. A **516**, 68 (2004).
- [5] A. Bettini *et al.*, Nucl. Instrum. Meth. A **305**, 177 (1991).
- [6] P.V.C Hough 'Method and means for recognizing complex patterns', United States Patent Office 3069654(1962)